INTERNATIONAL JOURNAL FOR NUMERICAL METHODS IN FLUIDS, VOL. 23, 1327–1345 (1996)

ONSET OF ASYMMETRY: FLOW PAST CIRCULAR AND ELLIPTIC CYLINDERS

MANOJ T. NAIR AND T. K. SENGUPTA

Department of Aerospace Engineering, Indian Institute of Technology, Kanpur 208 016, India

SUMMARY

A computational study of the development of two-dimensional unsteady viscous incompressible flow around a circular cylinder and elliptic cylinders is undertaken at a Reynolds number of 10,000. A higher-order upwind scheme is used to solve the Navier–Stokes equations by the finite difference method in order to study the onset of computed asymmetry around bluff bodies. For the computed cases the ellipses develop asymmetry much earlier than the circular cylinder. The receptivity of the computed flows in the presence of discrete roughness and surface vibration is studied. Finally, the role of discrete roughness in triggering asymmetry for flow past a circular cylinder is studied and compared with flow visualization experiments at $Re = 10{,}000$

KEY WORDS: unsteady flows; incompressible viscous flows; onset of asymmetry; Navier–Stokes equations; finite difference method; bluff bodies

1. INTRODUCTION

Bluff body aerodynamics has long been of interest to fluid dynamicists for both technological and scientific reasons. Such a flow, when started impulsively, is characterized by large-vorticity generation at the wall which is progressively convected and diffused for two-dimensional flows, with convection being dominant for the Reynolds number under consideration. The flow rapidly separates, forming a closed recirculation zone. In the early stages this zone is made up of two symmetric counter-rotating eddies. When the Reynolds number (based on diameter and freestream speed) exceeds 500, one can observe secondary and tertiary vortices in this early period of flow establishment. During this early period the wake bubble grows in width and length with time while retaining the symmetry up to a certain time. After this the eddies become asymmetrical and are shed alternately downstream to form a so-called Bénard–Kármán street. This time of asymmetry is primarily a function of Reynolds number and is facility-dependent; Honji and Taneda[1] report this time to be about eight for $Re = 200$. The flow visualization pictures at $Re = 10{,}000$ reported by Coutanceau and Defaye[2] indicate that this time is about four.

The periodic shedding of large-scale eddies from a bluff body placed in a uniform mean flow is one of the most common self-sustained oscillations in fluid mechanics. This is an open system and the above-mentioned behaviour occurs because of flow instability. There are numerous review articles on this topic, including those of Huerre and Monkewitz[3], Bearman and Graham,[4] Morkovin[5] and Oertel.[6] These are mostly concerned with the instability of laminar flows and are thus restricted to very low Reynolds numbers with special emphasis on local versus global instability and convective versus absolute instability. It has been observed by Huerre and Monkewitz[3] that flows past bluff

CCC 0271–2091/96/121327–19

Received June 1995
Revised February 1996

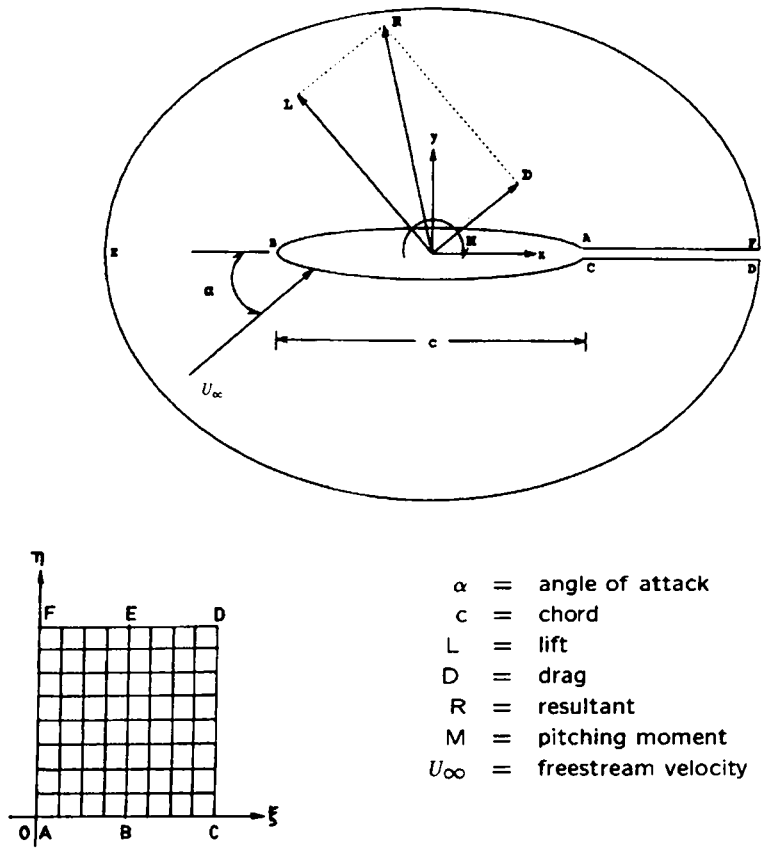

Figure 1. Physical and computational domain

bodies behave like an oscillator and the oscillator frequency as determined by vortex shedding is a complex combination of spatio–temporal growth of disturbances. By and large this explanation holds good for large Reynolds numbers also, but then one would be required to study the stability of mean flows, which are time-dependent. On the other hand, high-Reynolds-number flows have been studied for observing structural and topological changes by Dallman and Schewe[7] and Perry and Chong.[8] These studies emphasize that two-dimensional bubbles are unstable to a three-dimensional disturbance field, leading to a succession of bifurcations. The first bifurcation is the onset of asymmetry.

Therefore it is natural to capture the self-excited oscillations by means of directly computing the flow field by solving the three-dimensional unsteady Navier–Stokes equations. However, present-day computers do not allow such a simulation while resolving the necessary temporal and spatial scales. If the primary field is nominally two-dimensional, then it is possible to study the evolution of two-dimensional disturbances. In an earlier attempt, Hankey and Shang[9] have computed the flow field around a circular cylinder for a nominally two-dimensional flow. In this study no turbulence model was used for a flow at $Re = 1{\cdot}7 \times 10^5$. The instability of the inflectional point velocity distribution in the near wake showed two unstable modes, with the stronger one giving rise to asymmetric oscillation. This instability analysis is performed on the mean velocity wake profile. The asymmetric mode defines the Strouhal number, while the symmetric mode is associated with higher-frequency oscillation in the wake.

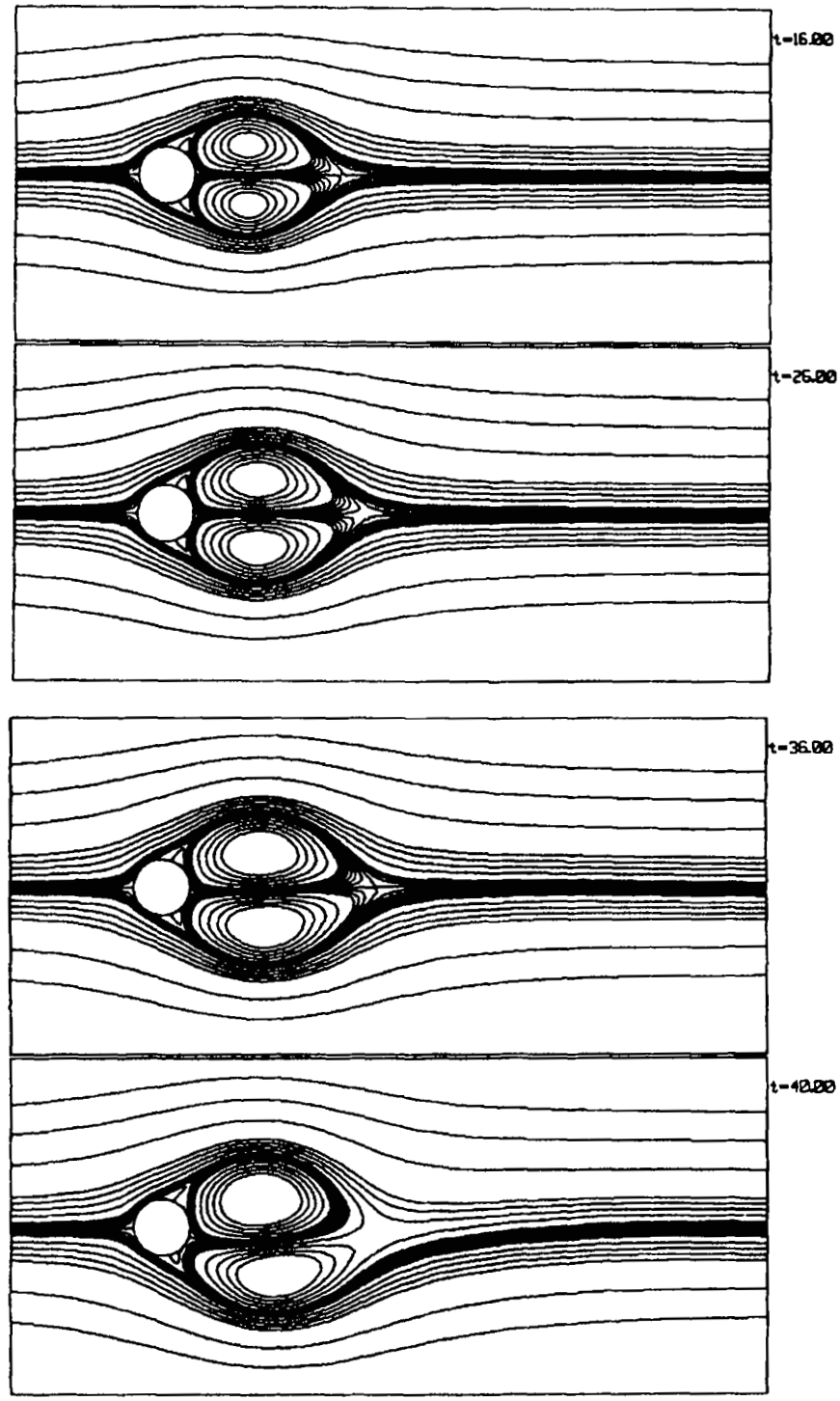

Figure 2. Streamline contours for circular cylinder at $Re = 10{,}000$

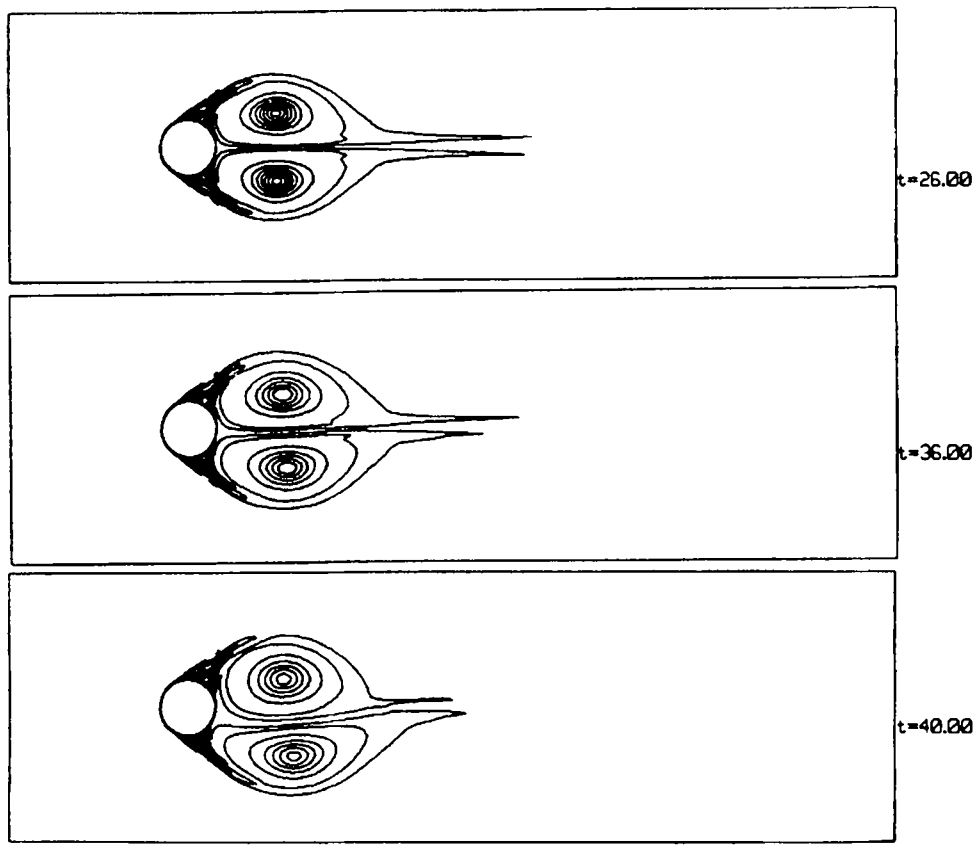

Figure 3. Vorticity contours for circular cylinder at $Re = 10{,}000$

While the simulation of Hankey and Shang[9] did produce asymmetry for the compressible code, various other investigations have reported the absence of asymmetry in their incompressible flow calculations (see e.g. Reference 10 and 11), where lower-order schemes are used. Braza *et al.*[10] have used a second-order scheme for their computations. In actual flow situations the loss of symmetry can be due to any combination of the following perturbation sources:

(a) non-uniform oncoming flow
(b) presence of surface roughness
(c) the running conditions of the experiment.

While it is appropriate to study such a flow development from the receptivity point of view, the disturbance environment cannot always be prescribed.

In the present work we have concentrated on studying the onset of asymmetry in the near wake of a circular cylinder and elliptic cylinders of various thickness/chord ratios. While it is necessary to trigger asymmetry for the case of the circular cylinder to compare with experiments, asymmetry develops quickly for the flow past elliptic cylinders. A nominally two-dimensional flow past a circular cylinder maintains its symmetry for a long time because of the absence of a preferred direction in the computational field. It has been shown that the asymmetry can be triggered easily by either a transverse surface vibration or discrete roughness element. Finally, the flow past a circular cylinder at $Re = 10{,}000$ is simulated and compared with experimental results when asymmetry is triggered by surface roughness.

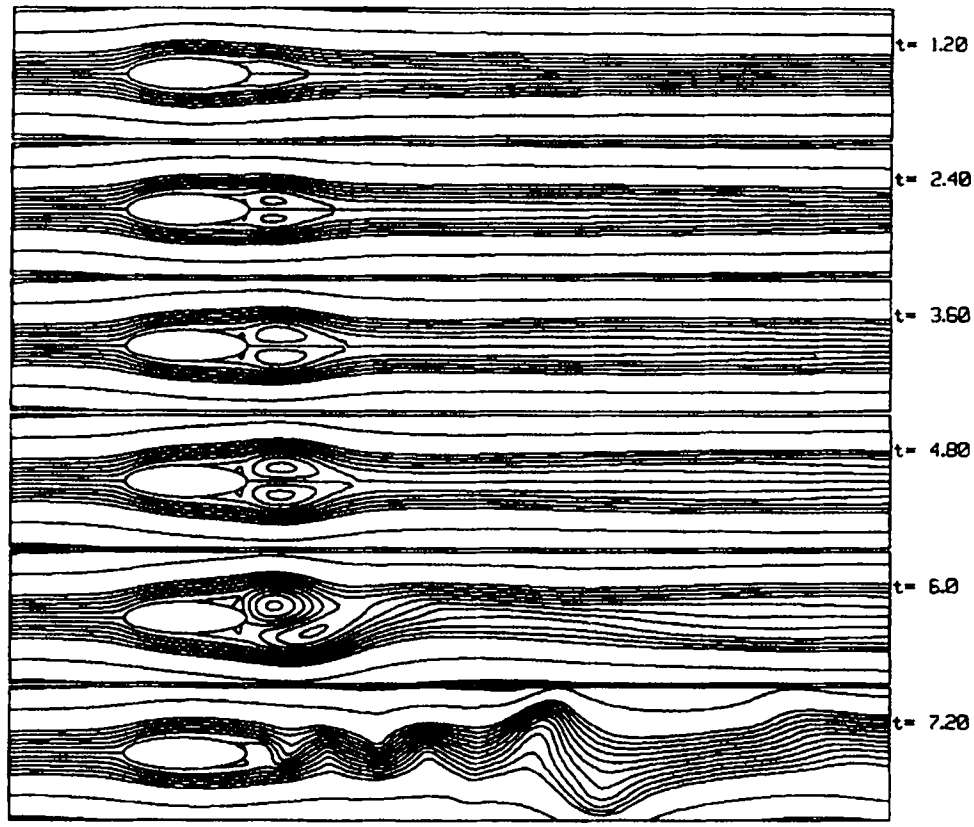

Figure 4. Streamline contours for elliptic cylinders of $t/c = 0{\cdot}25$ at $Re = 10{,}000$

In the next section the formulation of the problem is given. Results and discussion are given in Section 3 and this is followed by conclusions.

2. FORMULATION

The unsteady incompressible two-dimensional Navier–Stokes equations are solved in the streamfunction–vorticity formulation

$$\vec{\nabla}^2\psi = -\omega, \tag{1}$$

$$\frac{\partial\omega}{\partial t} + \nabla\cdot(\omega\vec{V}) = \frac{1}{Re}\vec{\nabla}^2\omega, \tag{2}$$

where ψ is the streamfunction given by

$$\vec{V} = \vec{\nabla}\times\psi \tag{3}$$

and ω is the only component of vorticity for the two-dimensional flow, given by

$$\omega = |\vec{\nabla}\times\vec{V}|\hat{k}. \tag{4}$$

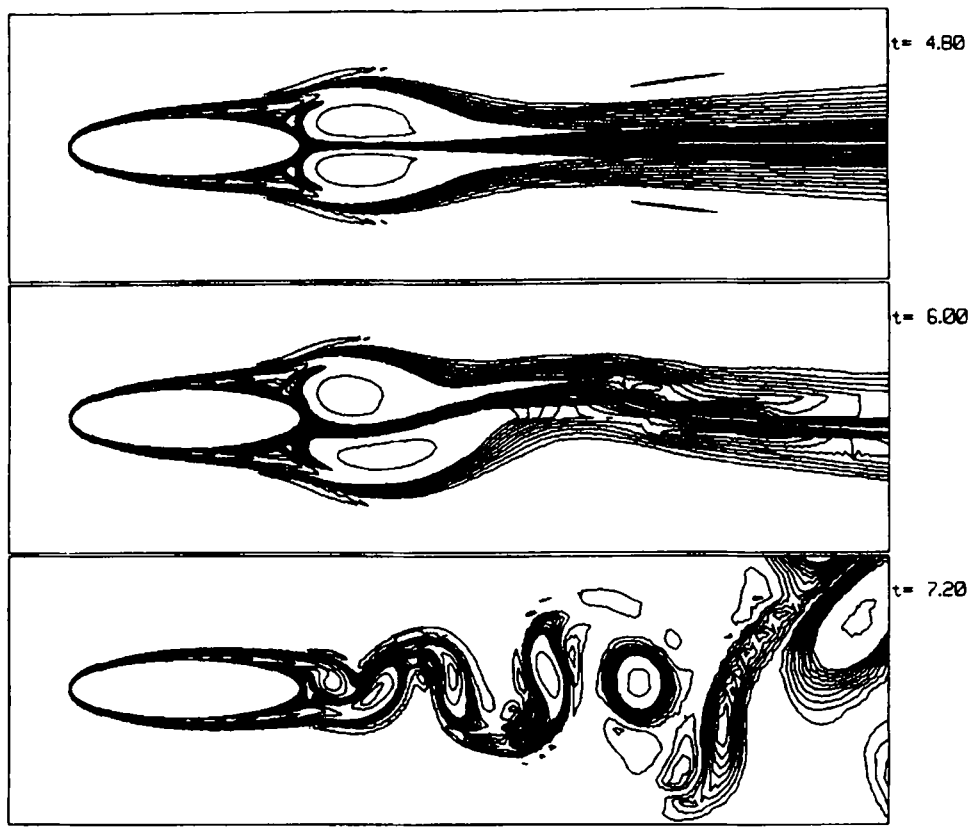

Figure 5. Vorticity contours for elliptic cylinder of $t/c = 0{\cdot}25$ at $Re = 10{,}000$

All lengths are non-dimensionalized with respect to the diameter/chord of the circular/elliptic cylinder. The velocity scale used is the freestream speed. The time scale is defined by these length and velocity scales.

Equations (1) and (2) are solved in an orthogonal transformed plane (Figure 1). The governing equations in the transformed plane are given by

$$\frac{\partial}{\partial \xi}\left(\frac{h_2}{h_1}\frac{\partial \psi}{\partial \xi}\right) + \frac{\partial}{\partial \eta}\left(\frac{h_1}{h_2}\frac{\partial \psi}{\partial \eta}\right) = -h_1 h_2 \omega, \tag{5}$$

$$h_1 h_2 \frac{\partial \omega}{\partial t} + h_2 u \frac{\partial \omega}{\partial \xi} + h_1 v \frac{\partial \omega}{\partial \eta} = \frac{1}{Re}\left[\frac{\partial}{\partial \xi}\left(\frac{h_2}{h_1}\frac{\partial \omega}{\partial \xi}\right) + \frac{\partial}{\partial \eta}\left(\frac{h_1}{h_2}\frac{\partial \omega}{\partial \eta}\right)\right], \tag{6}$$

where h_1 and h_2 are the scale factors of the transformation. The contravariant components of velocity in the transformed plane are given by

$$u = \frac{1}{h_2}\frac{\partial \psi}{\partial \eta}, \qquad v = -\frac{1}{h_1}\frac{\partial \psi}{\partial \xi}. \tag{7}$$

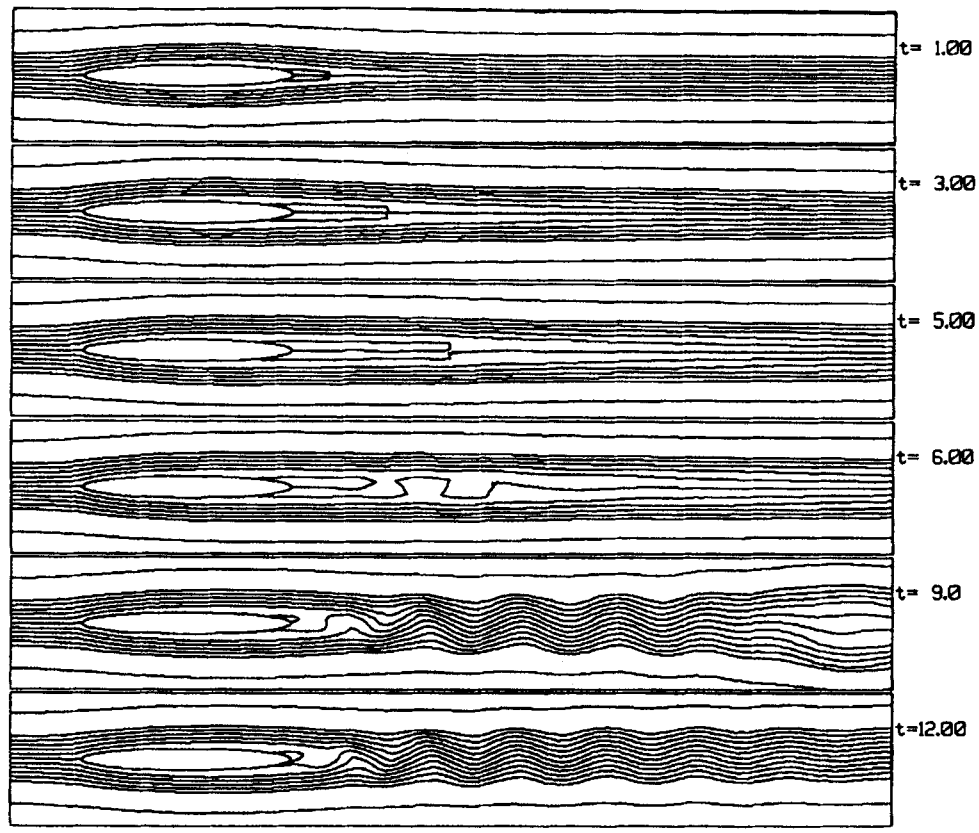

Figure 6. Streamline contours for elliptic cylinders of $t/c = 0{\cdot}1$ at $Re = 10{,}000$

The analytical orthogonal transformation used for the circular cylinder is given by

$$x = r(\eta)\cos(2\pi\xi), \qquad y = r(\eta)\sin(2\pi\xi), \tag{8}$$

with uniform spacing in the azimuthal direction (ξ). The grid is stretched in the radial direction (η) and is given by

$$r(\eta) = r_0 + \frac{\eta}{\Delta\eta}\left[\Delta r_0 + \frac{d}{2}\left(\frac{\eta}{\Delta\eta} - 1\right)\right], \tag{9}$$

where r_0 is the radius of the cylinder, Δr_0 is the spacing between the cylinder and the first concentric grid line and d is the increment of successive concentric grid line spacings. Other details of the formulation are the same as in Reference 12.

In the case of an elliptic cylinder the orthogonal transformation is given by

$$x = a\ \cos(2\pi\xi)\cosh[(\eta_2 - \eta_1)\eta + \eta_1], \qquad y = a\sin(2\pi\xi)\sinh[(\eta_2 - \eta_1)\eta + \eta_1], \tag{10}$$

where a is the focal distance, $\eta = \eta_1$ is the ellipse and $\eta = \eta_2$ is the outer boundary.

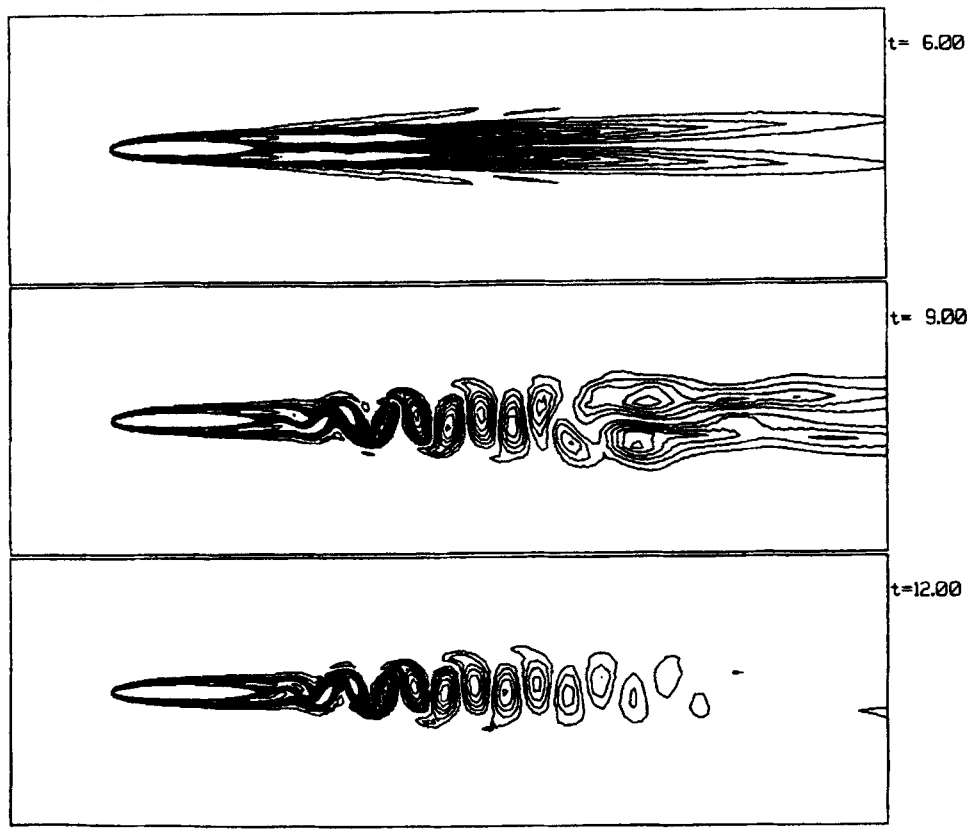

Figure 7. Vorticity contours for elliptic cylinder of $t/c = 0{\cdot}1$ at $Re = 10{,}000$

Boundary and initial conditions (referring to Figure 1)

On the solid boundary (ABC) the no-slip condition is applied:

$$\psi = \text{constant}, \qquad \partial\psi/\partial\eta = 0. \tag{11}$$

This condition fixes the wall vorticity as

$$\omega_b = -\frac{1}{h_2^2}\frac{\partial^2\psi}{\partial\eta^2}\bigg|_{\text{wall}}. \tag{12}$$

A periodic boundary condition is applied at the cut (AF and CD). At the outer boundary (DEF), uniform flow conditions are applied. The far-field boundary condition used for the vorticity transport equation (6) is

$$\partial\omega/\partial\eta = 0. \tag{13}$$

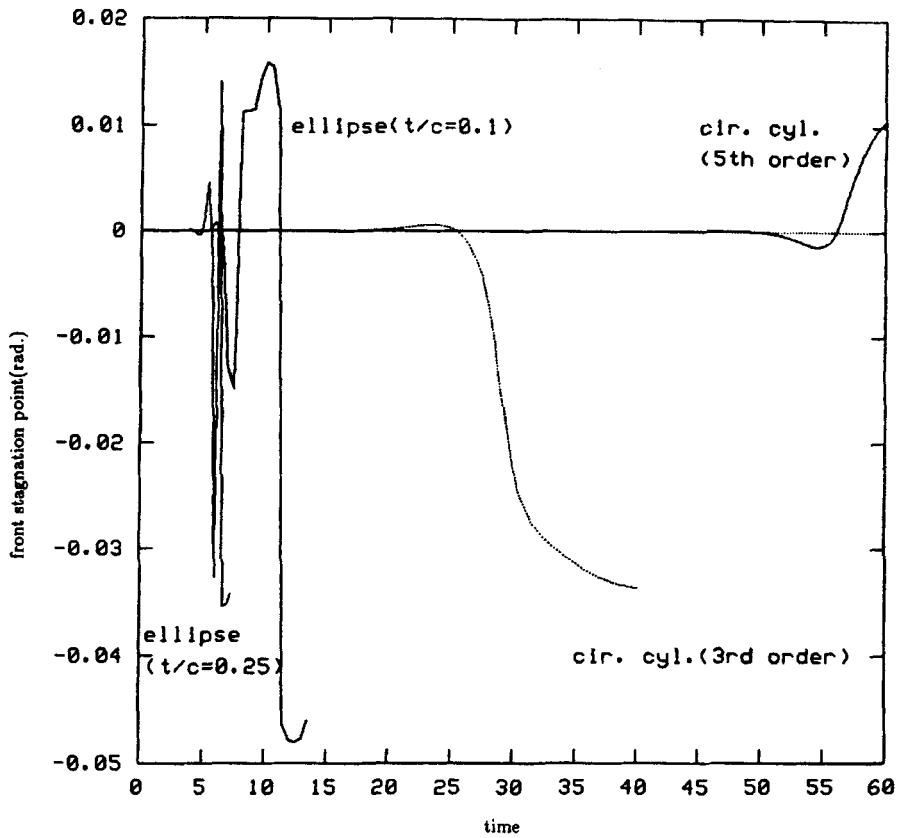

Figure 8. Front stagnation point versus time for circular cylinder and elliptic cylinders of $t/c = 0{\cdot}1$ and $0{\cdot}25$

Equations (5) and (6) are solved using the finite difference technique. Equation (5) is solved using an alternating direction implicit (ADI) method due to Peaceman and Rachford, given in Reference 13. The iterations are continued till the solution residue at every point is reduced to 10^{-5}. Equation (6) is solved using an explicit Euler backward scheme for time discretization. Central differencing is used for the diffusion terms, while a third-order upwind scheme developed by Kawamura *et al.*[14] is used for the convection terms. This discretization for convection terms has a truncation error proportional to the fourth derivative with respect to the transformed variable.

The problem under investigation is to study the onset of asymmetry after the flow is impulsively started. Hence the initial condition is given by inviscid irrotational flow.

Additionally, pressure information in the complete flow field is obtained by solving the Poisson equation for pressure given by

$$\nabla^2 p = \frac{\partial v\omega}{\partial \xi} - \frac{\partial u\omega}{\partial \eta}. \tag{14}$$

In the orthogonal transformed plane, equation (14) is given by

$$\frac{\partial}{\partial \xi}\left(\frac{h_2}{h_1}\frac{\partial p}{\partial \xi}\right) + \frac{\partial}{\partial \eta}\left(\frac{h_1}{h_2}\frac{\partial p}{\partial \eta}\right) = \frac{\partial}{\partial \xi}(h_2 v\omega) - \frac{\partial}{\partial \eta}(h_1 u\omega). \tag{15}$$

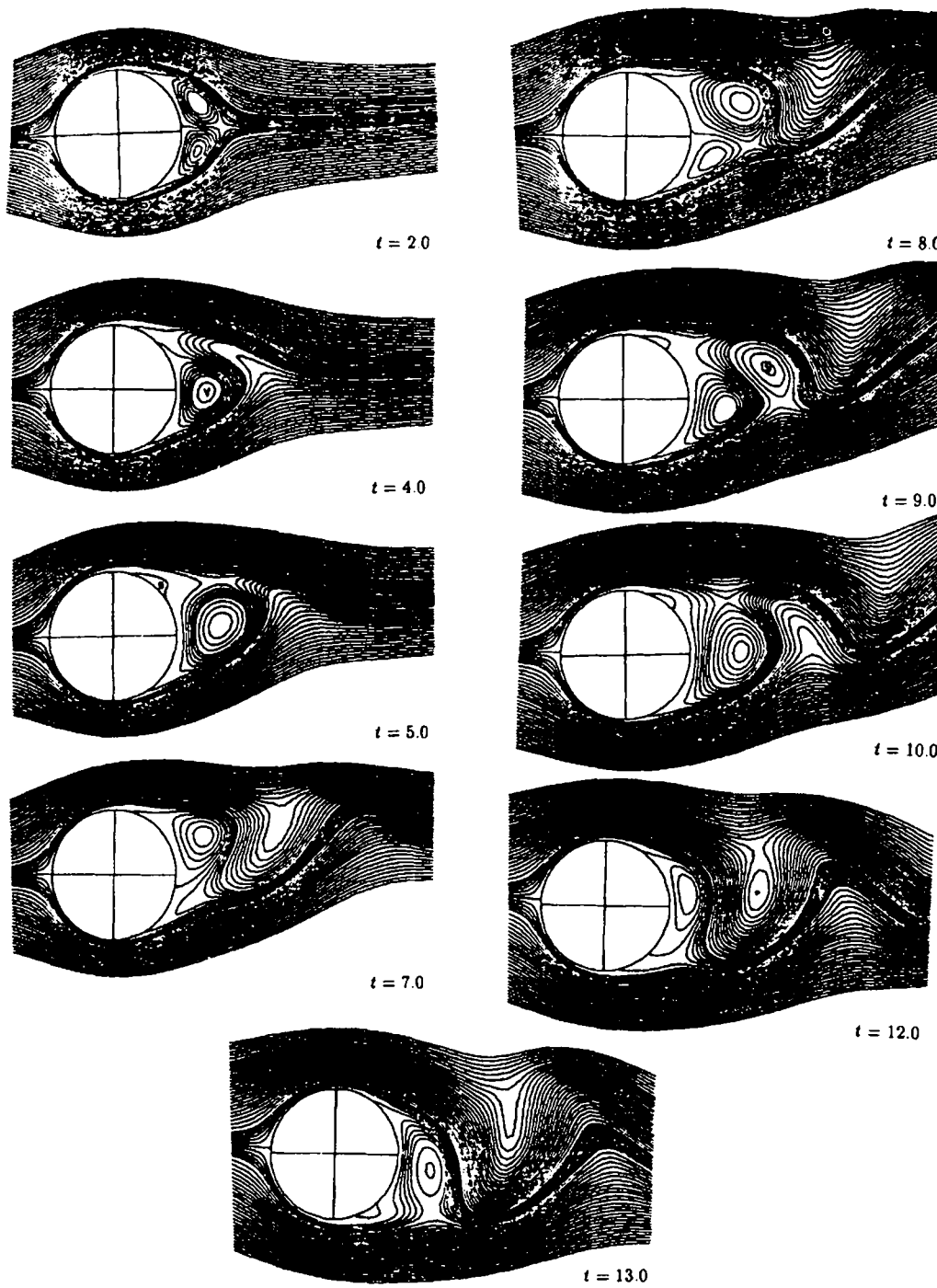

Figure 9. Streamline contours for translating and obliquely oscillating circular cylinder at $Re = 200$

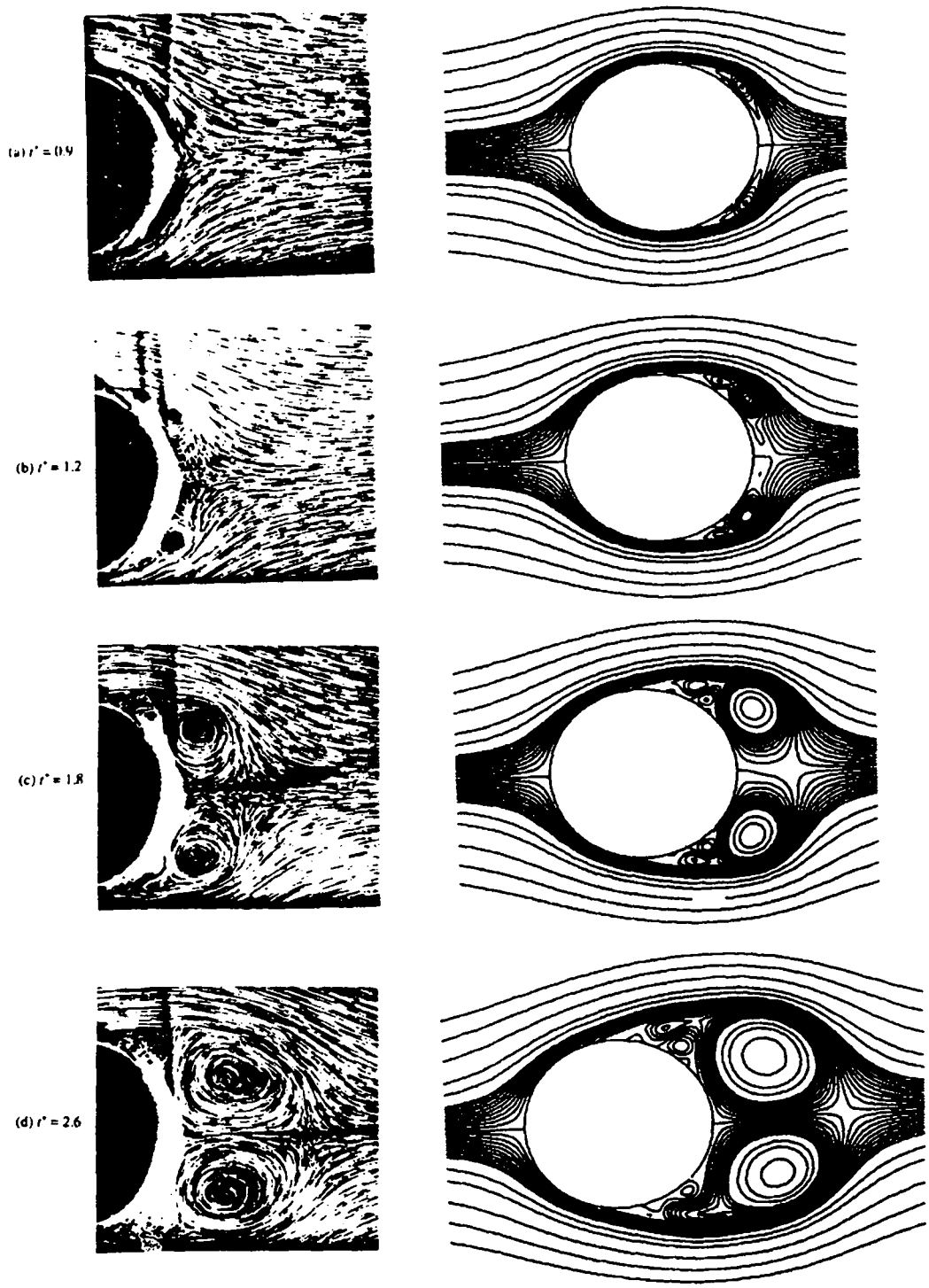

Figure 10. (a)–(d) Streamline contours for circular cylinder with roughness at $Re = 10{,}000$

A Neumann boundary condition at the surface and far stream, as obtained from the normal momentum equation, is used in solving equation (15) along with the periodic condition on the cut.

3. RESULTS AND DISCUSSION

All the computations are done for $Re = 10{,}000$ with an initial time step of 10^{-4} which was increased 10-fold after $t = 4$. We have also computed the flow past a circular cylinder with second-order time accuracy (three-point backward scheme) for $Re = 9500$ and compared it with results presented in Reference 12. Since there were no significant changes in the results, all the cases were computed with the Euler backward scheme.

The present method has also been used to compute the flow field past a rotating and translating cylinder for various combinations of rotation speed and Reynolds number. The results presented in Reference 15 compared excellently with available experimental results. All these points to the accuracy of the results presented herein.

For the circular cylinder case, 251 points are taken in the azimuthal (ξ) direction and 300 points in the radial (η) direction, where the outer boundary is more than 36 diameters away in a O-type grid. For all the computations the first grid line in the radial direction is 10^{-3} of the diameter/chord of the circular/elliptic cylinder. The grid is expanded in a smooth way such that the dispersion and dissipation errors are minimized.[15]

Figure 2 shows the computed streamlines for the flow past a circular cylinder up to the non-dimensional time $t = 40$. The vorticity contours for later times, as presented in Figure 3, clearly show the asymmetry. These figures show that the flow remains symmetric up to $t = 26$. Similar symmetry was previously observed by Son and Hanratty,[16] Martinez[11] and Braza *et al.*[10] Braza *et al.*[10] have said that *the flow always achieves a steady symmetric pattern after a longer or shorter establishment period* for $Re = 1000$. However, the authors contradict this later by saying that in a numerical simulation, although the destabilizing perturbation sources are absent, the truncation and round-off errors will trigger asymmetry after a large computing time. Figure 2 shows asymmetry developing first at $t = 26$ when one of the wake bubbles opens up in the downstream direction and a streamline which is outside the other attached bubble wraps around the released bubble to form an *alleyway*. This opens up further as time progresses and the first vortex is released at $t = 40$. This can be explained by noting that the present higher-order scheme has much lower phase errors for high-wave-number components as compared with the lower-order schemes used by Braza *et al.*[10] and Martinez.[11] The lower-order schemes filter out the higher-wave-number components which are responsible for triggering asymmetry.

Next, when the same solver was used to compute the flow field past an elliptic cylinder of thickness/chord ratio 0·25 for the same Reynolds number, the flow field became asymmetric around $t = 4{\cdot}8$. This can be easily seen in the streamfunction contours in Figure 4 and the vorticity contours in Figure 5.

The flow field around an elliptic cylinder of thickness/chord ratio 0·1 at zero angle of attack was then computed (Figures 6 and 7). Aerodynamically this is akin to a streamlined body such as an aerofoil. From the streamline contours plotted in Figure 6, it is evident that the flow becomes asymmetric around $t = 5$. However, in this case the asymmetry and near-wake phenomena are different in nature. The symmetric wake bubble in this case is longer compared with the other cases and this elongated bubble suffers an instability of Kelvin–Helmhotz type and breaks into oscillatory wavy flow in the wake. If one attempts to measure an equivalent Strouhal number, this will be large compared with that of a circular cylinder, which is also found experimentally by Modi and Wiland[17] and Ota *et al.*[18] Thus computationally the onset of asymmetry is function of eccentricity of the body

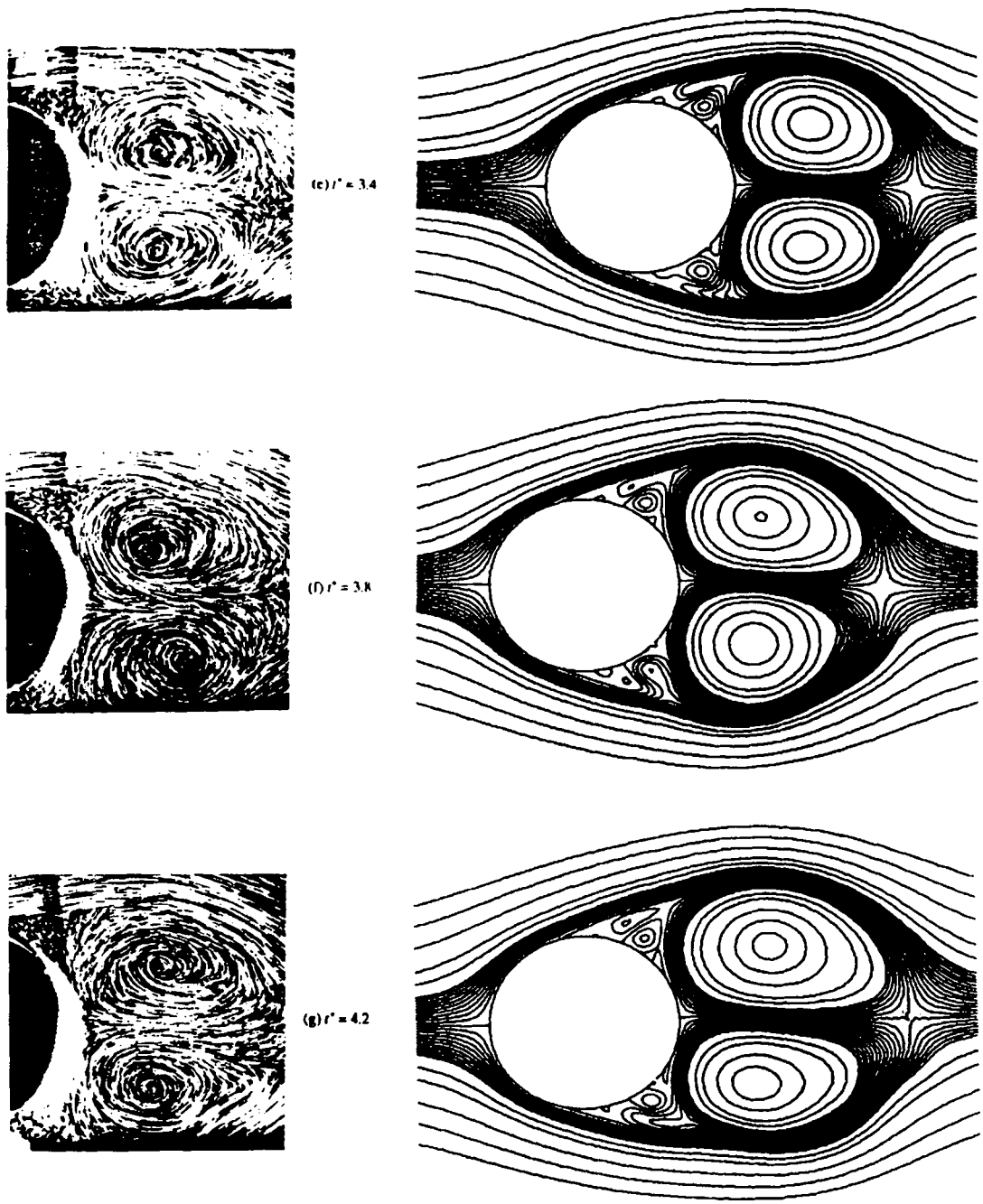

Figure 10. (e)–(g) Streamline contours for circular cylinder with roughness at $Re = 10{,}000$

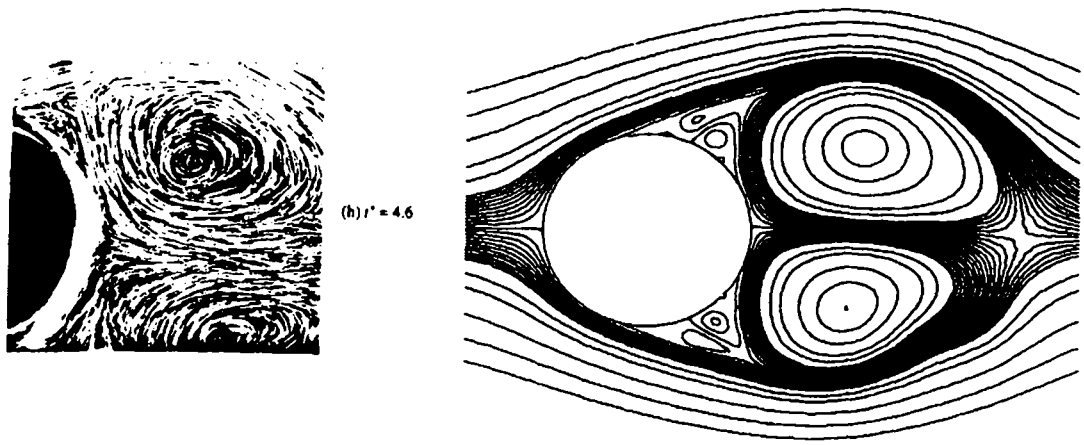

Figure 10. (h) Streamline contours for circular cylinder with roughness at $Re = 10{,}000$

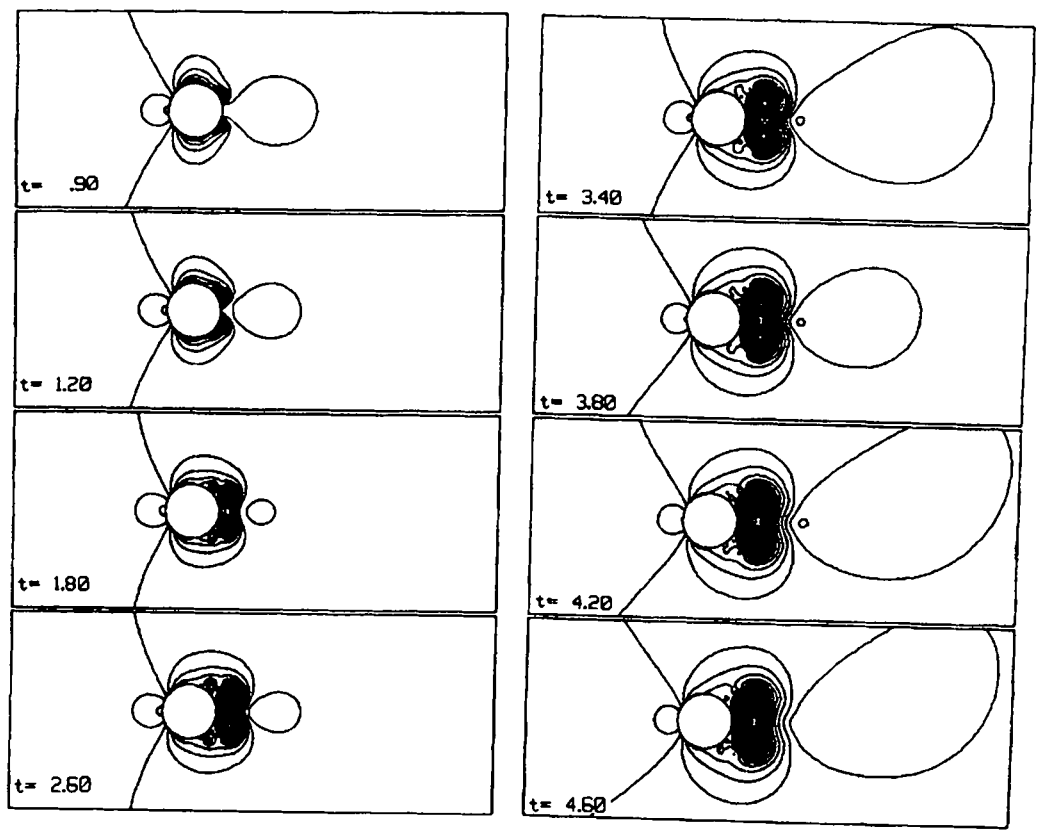

Figure 11. Pressure contours for circular cylinder with roughness at $Re = 10{,}000$

or, more precisely, the streamline curvature near the trailing edge. It can be reasoned that bodies with sharp corners, such as rectangular or square cylinder, will exhibit even earlier onset of asymmetry. To explain this, one should note that a circular cylinder has perfect symmetry with identical body curvature everywhere. In this sense the circular cylinder is special, and when the outer boundary is also a concentric circle, the flow does not have a preferred direction. Any small changes impressed upon the circular cylinder flow field cause the front and rear stagnation points to move in such a fashion that eventually symmetry prevails, while for an ellipse there is a preferred direction along with varying radius of curvature of the body. In Figure 8 we have shown the departure of the front stagnation point with respect to its initial location as a function of time. It is well known that the front stagnation point always moves about its initial location for high-Reynolds-number flows and it is the stability property of the near wake which transmits the disturbance quantities in incompressible flow to the front stagnation point. Figure 8 is thus an indicator of flow instability of the near wake to very small perturbations. This figure represents the receptivity of the flow field around circular and elliptic cylinders to numerical disturbances. The figure shows that the disturbance field, after a quiescent period of flow development, initially grows exponentially as a function of time. For the elliptic cylinders the onset of asymmetry occurs at around the same time, but for the thicker ellipse the instability frequency is larger than that for the slender ellipse. Also, comparison of the two ellipse cases reveals that the non-linear temporal growth is very important for the slender ellipse—one can see a non-linear saturation of disturbance after only one cycle.

In the same figure we have shown the numerical onset of asymmetry for a circular cylinder using a fifth-order upwind scheme for the vorticity transport equation. The delayed onset of asymmetry for this case as compared with third-order scheme once again demonstrates the fact that the circular cylinder flow field is sensitive to accumulation of numerical error.

Next we investigated the receptivity of the flow past a circular cylinder to surface vibration. Figure 9 shows the streamline contours up to $t = 13$ for the flow field around a circular cylinder which executes oscillation in an oblique direction at $Re = 200$. Once again it is seen that the symmetry of the flow is lost very early (at $t = 2$) for very small oscillations even at this low value of Reynolds number. The cylinder vibrates according to

$$\vec{r}_b = -a_x \cos(\omega_x t)\hat{i} - a_y \cos(\omega_y t)\hat{j}, \tag{16}$$

where $\hat{i}$ and $\hat{j}$ are the unit vectors along the direction x and y respectively. The reported results are obtained with a 121×150 grid with a very small time step of 5×10^{-5} by an explicit procedure. The parameters of vibration are given by

$$a_x = 0{\cdot}25, \qquad a_y = 0{\cdot}25, \qquad \omega_x = \omega_y = \pi.$$

These results are in conformity with the findings of Hankey and Shang.[9] It was shown by Hankey and Shang[9] that the asymmetric mode is more unstable than the symmetric mode. By oscillating the cylinder in the horizontal direction, one suppresses the asymmetric mode, while small transverse oscillation triggers asymmetry very quickly, as the disturbance growth rates are very high for the asymmetric mode as compared with the symmetric mode.

It should be pointed out that to the best of our knowledge there are no computations available for flow past an elliptic cylinder at $Re = 10,000$. Lugt and Haussling[20] have studied the flow past an elliptic cylinder at Reynolds numbers of 15, 30 and 200 with the cylinder fixed at an angle of attack of 45°. Ohmi *et al.*[21] have done both experimental and computational studies of the dynamic stall of

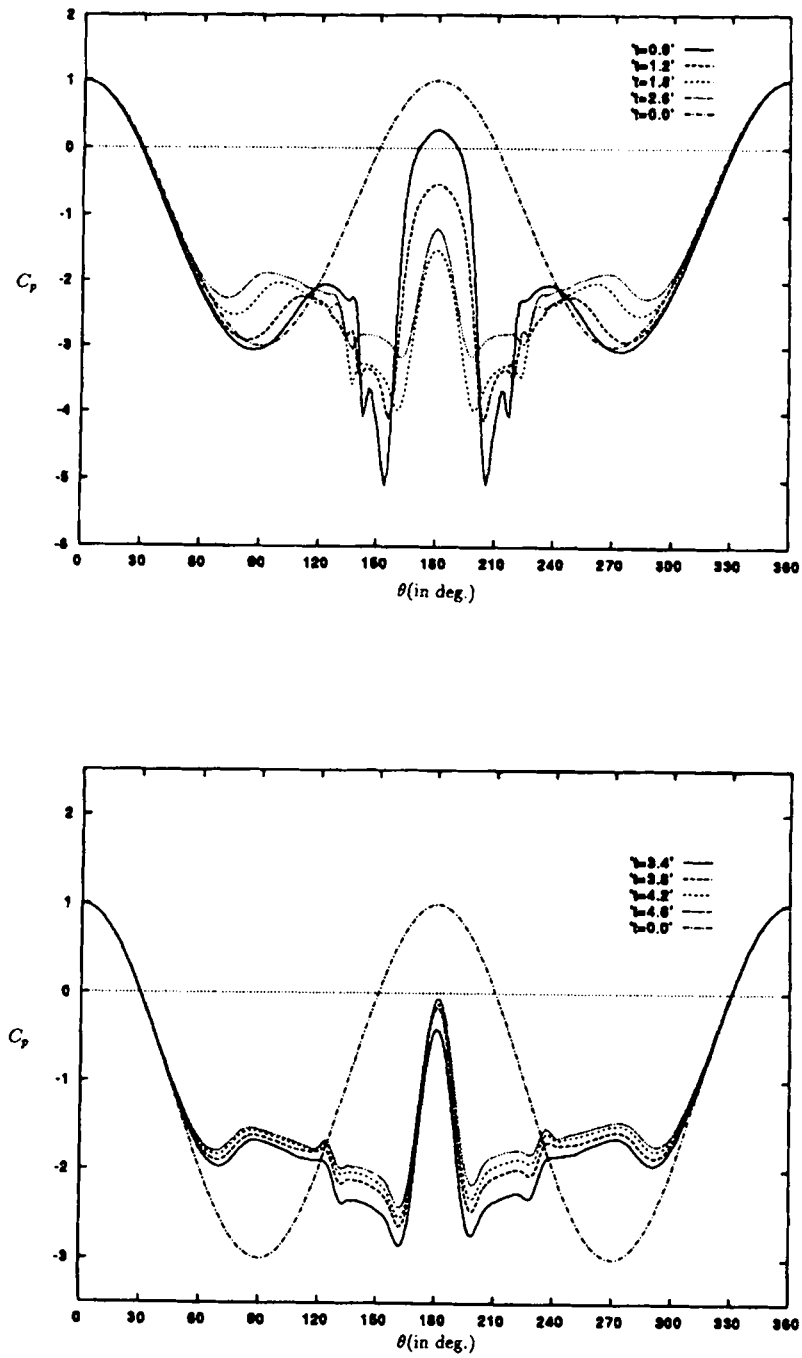

Figure 12. C_p distribution on surface of circular cylinder with roughness at $Re = 10{,}000$

an elliptic aerofoil. Most of the results are for $Re = 3000$ with various frequency parameters. Here we have shown only the results for zero angle of attack. Detailed results giving the flow field around elliptic aerofoils for a range of angles of attack will be presented elsewhere.

Finally, the flow field is computed around a circular cylinder with asymmetry induced by localized surface roughness and the results are compared with experimental visualization pictures of Coutanceau and Defaye.[2] As mentioned earlier, the onset of asymmetry in actual flows could be due to multiple reasons and here we have chosen surface roughness as was done by Kawamura *et al.*[14] This method is much more realistic than what has been done by Braza *et al.*[10] and Martinez[11] where a doublet-type disturbance is provided by rotating the cylinder in clockwise and anticlockwise directions successively. The establishment period even with the chosen strategy is an order of magnitude higher than in actual flows. We have shown the computed and experimental instantaneous streamline at some fixed time instants. It is easy to see from the experimental visualization pictures that the flow shows early asymmetry at $t = 3{\cdot}8$. The corresponding computed streamline contours are shown in Figure 10.

The roughness element has to be localized and asymmetrically placed on the surface. Statistically this is equivalent to the skewness of the roughness distribution. For a purely *random* rough surface the mean is zero, while the second-order statistics add to the *melt height* everywhere and it is the third-order statistics which produces asymmetry. The computed results with chosen roughness indicate that the roughness size to trigger asymmetry is of the order of 0·6% of the diameter. The roughness element is located at 138° with respect to the front stagnation point. Thus this is located within the recirculation zone. It should be noted that the roughness is only effective when placed in a zone after the point of separation. The asymmetric disturbance when produced before the point of separation is damped strongly and one would require a larger roughness size to achieve the same purpose.

Figure 11 shows the pressure distribution in the complete field after the impulsive start. The contours drawn are in the range from $-8{\cdot}0$ to $1{\cdot}5$ at intervals of 0·5. The development of flow around the cylinder and the beginning of asymmetry can be noticed. Figure 12 shows the C_p distribution on the circular cylinder at various times. It can be noticed that C_p at $\theta = 150$ deg for the initial times are much lower than the minimum inviscid C_p. This is due to the high velocity induced near the surface by the vortex which has just formed quite close to the cylinder. This results in a high value of C_d at the start as shown in Figure 13. The initial high C_d is also observed by Braza *et al.*[10] in their computations at $Re = 1000$.

4. CONCLUSIONS

In this paper the onset of asymmetry is studied for a circular cylinder and elliptic cylinders. While the circular cylinder flow field remains symmetric for a long time, the flow field around the elliptic cylinders at zero incidence become asymmetric earlier. Furthermore, for the ellipses the asymmetry starts at the same time for both cases considered, but the asymmetry develops at a faster rate for the thicker ellipse. However, as the thickness/chord ratio is reduced, the asymmetry is due to the Kelvin–Helmholtz-type instability of the wake bubble by high-wave-number disturbances.

Also studied is the way to introduce asymmetry in the flow field by surface vibration and localized roughness. A detailed comparison with experimental visualizations of the flow field past a circular cylinder at $Re = 10,000$ is made when the asymmetry is triggered by localized surface roughness. The flow is established early when the roughness is located in the zone where the shear layer is separated and the roughness height has a minimum value above which the flow establishment process follows the experimental value.

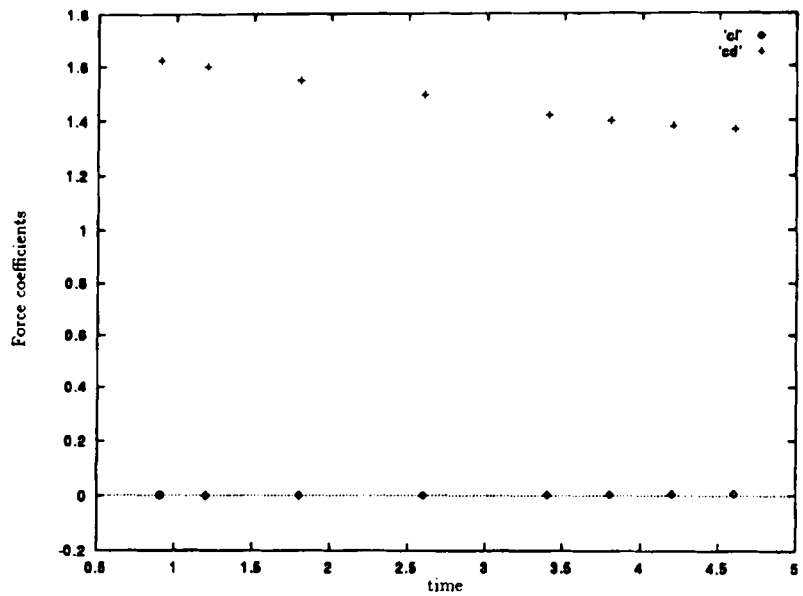

Figure 13. Lift and drag coefficients as a function of time for circular cylinder with roughness at $Re = 10{,}000$

All these studies relate to two-dimensional disturbances. It would be natural to study a three-dimensional flow field even though the primary field is nominally two-dimensional.

ACKNOWLEDGEMENTS

The authors would like to acknowledge the help provided by Sandeep Kothari in computing the flow field past an oscillating cylinder (Figure 9). We would also like to record our appreciation to Umendra Singh Chauhan for his help with the graphics. This work was done as part of a sponsored project funded by the Aeronautical Research and Development Board (ARDB) and the authors acknowledge the support and especially the interest and encouragement shown by Dr. T. S. Prahlad.

REFERENCES

1. H. Honji and S. Taneda, 'Unsteady flow past a circular cylinder', *J. Phy. Soc. Jpn.*, **27**, 1668–1677 (1969).
2. M. Coutanceau and J. R. Defaye, 'Circular cylinder wake configuratons: a flow visualization survey', *Appl. Mech. Rev.*, **44**(6), 225–305 (1991).
3. P. Huerre and P. A. Monkewitz, 'Local and global instabilities in spatially developing flows', *Ann. Rev. Fluid Mech.*, **22**, 473–538 (1990).
4. P. W. Bearman and J. M. R. Graham, 'Vortex shedding from bluff bodies in oscillatory flow: a report on Euromech 119', **99**, *J. Fluid Mech.*, 225–245 (1980).
5. M. V. Morkovin, 'Recent insights into instability and transition', *AIAA Paper 88-3675*, 1988.
6. H. Oertel, Jr., 'Wakes behind blunt bodies', *Ann. Rev. Fluid. Mech.*, **22**, 539–564 (1990).
7. U. Dallman and G. Schewe, 'On topological changes of separating flow structures at transition Reynolds number', *AIAA Paper 87-1266*, 1987.
8. A. E. Perry and M. S. Chong, 'A description of eddying motions and flow patterns using critical point concepts', *Ann. Rev. Fluid Mech.*, **19**, 125–155 (1987).
9. W. L. Hankey and J. S. Shang, 'Numerical simulations of self-excited oscillations in fluid flows', in W. G. Habashi (ed.), *Computational Methods in Viscous Flows, Vol. 3*, Pineridge, Swansea, 1984, pp. 543–582.
10. M. Braza, P. Chassaing and H. Ha Minh, 'Numerical study and physical analysis of the pressure and velocity fields in the near wake of a circular cylinder', *J. Fluid. Mech.*, **165**, 79–130 (1986).

11. G. Martinez, *Thèse Docteur-Ingénieur*, INP, Tolouse, 1979.
12. T. K. Sengupta and R. Sengupta, 'Flow past an impulsively started circular cylinder at high Reynolds number', *Comput. Mech.*, **14**, 298–310 (1994).
13. W. F. Ames, *Numerical Methods for Partial Differential Equations*, Academic, New York, 1992.
14. T. Kawamura, H. Takami and K. Kuwahara, 'New higher order upwind scheme for incompressible Navier–Stokes equations', *Fluid Dyn. Res.*, **1**, 145–162 (1985).
15. T. K. Sengupta, U. S. Chauhan and M. T. Nair, 'Flow past a translating and spinning cylinder', *Comput. Fluids*, submitted.
16. J. S. Son and T. J. Hanratty, 'Numerical solution of the flow around a cylinder at Reynolds number of 40, 200, 500', *J. Fluid Mech.*, **35**, 369–386 (1969).
17. V. J. Modi and E. Wiland, 'Unsteady aerodynamics of stationary elliptic cylinders in subcritical flow', *AIAA J.*, **8**, 1814–1821 (1970).
18. T. Ota, H. Nishiyama and Y. Taoka, 'Flow around an elliptic cylinder in the critical Reynolds number regime', *J. Fluids Eng.*, **109**, 149–155 (1987).
19. C. P. Jackson, 'A finite-element study of the onset of vortex shedding in flow past variously shaped bodies', *J. Fluid Mech.*, **182**, 23–45 (1987).
20. H. J. Lugt and H. J. Haussling, 'Laminar flow past an abruptly accelerated elliptic cylinder at 45° incidence', *J. Fluid Mech.*, **65**, 711–734 (1974).
21. K. Ohmi, M. Coutanceau, L. Ta Phuoc and A. Dulieu, 'Vortex formation around an oscillating and translating airfoil at large incidences', *J. Fluid Mech.*, **211**, 37–60 (1990).